ISBN: 978-3-95450-227-1 ISSN: 2673-5490 doi:10.18429/JACoW-IPAC2022-MOPOMS027

SYNTHESIS OF FIRST CAESIUM TELLURIDE PHOTOCATHODE AT ASTEC USING SEQUENTIAL AND CO-DEPOSITION METHOD.

R. Valizadeh, A.N. Hannah, STFC, WA4 4AD Warrington, UK
V.R. Dhanak, The University of Liverpool, L69 7ZF Liverpool, UK

Abstract

Caesium Telluride (Cs_2Te) photocathodes, are the electron source of choice, by many global accelerators such as European XFEL, FLASH and AWA. It offers high quantum efficiency and reasonable operational lifetime with lower vacuum requirements than multi-alkali photocathodes.

In this paper, we report on the first synthesised Cs_xTe photocathodes at ASTeC, using both sequential and co-deposition of Te and Cs on Mo substrate. Te deposition is carried out using ion beam deposition whilst the Cs is deposited using a SAES getter alkali. The ion beam deposition of Te provides a high degree of control to give a dense, smooth layer with a reproducible film thickness. The chemical state with respect to film composition of the deposited Cs_xTe is determined with in-situ XPS analyses. The films exhibit a quantum efficiency between 7.5 to 9% at 266 nm wavelength.

INTRODUCTION

The performance of a FEL is strongly related to the brightness of the electron beam generated by the photocathode. Hence, the performance of the cathode will be strongly dependent on its preparation, prior to its installation in the gun. The Linear accelerator CLARA [1], currently under development at the STFC Daresbury Laboratory will eventually drive a FEL facility in the future. At the commissioning stage, CLARA's Front End photo injector, is based on a 2.5 cell S-band photocathode RF gun, operating with a copper photocathode and driven by the third harmonic of a Ti: Sapphire laser (266 nm). It is installed in a dedicated thermally stabilized room. Light pulses with energies of up to 85 μJ are focused to a spot size of 1 mm with a timing length currently varying from 2 to 20 ps FWHM and a repetition rate of 10 Hz (eventually 400 Hz). Two class of photocathode types are envisaged to be used in CLARA mainly metallic or semiconductor.

Metallic photocathodes offer several clear advantages over semiconductor photocathodes. First, they are the most robust photocathodes against degradation caused by surface contamination and therefore do not require ultra-high vacuum conditions [1] and they can be cleaned inside the RF-gun. Second, they are robust against damage resulting from conditioning or heating. In addition, they can withstand high electric surface fields, such as those present at the cathode in RF accelerators, while other types of photocathode materials may suffer from electric breakdown. Other advantages of metallic photocathodes are their very short response time (less than picoseconds) and their very long lifetime (years or longer), which is much longer than other types of photocathodes. However, the main problem with metallic photocathodes is the rather low quantum efficiency (QE), even for UV radiation. This is due to their high reflectivity, and shallow escape depth due to electron-electron scattering. Semiconductor photocathodes have a much higher QE than metallic photocathodes, reaching values in the order of 10%. However, the lifetime is much shorter. The lifetime for semiconductor photocathodes is usually defined as the (operational) time over which the QE remains larger than 1% [2]. Another disadvantage is their high sensitivity to contamination by oxygen, CO_2 and water, which requires working in more stringent ultra-high vacuum conditions. Moreover, the response time is longer, typically in the range of tens of picoseconds. Alkali-telluride photocathodes have larger QE's and longer operational lifetimes than alkali-antimonide photocathodes. In addition, they offer the possibility of partial rejuvenation by means of heating. Among the alkali-telluride photocathodes, Cs_2Te is the most widely used one because of its relatively long potential lifetime (up to months [3]) and high QE compared to other semiconductor photocathodes [4-9]. A QE of 8 – 12% is consistently obtained at illumination with ~262 nm radiation under operational conditions (usually this means applying an RF field on the cathode while illuminating it with laser pulses, in 10^{-9} Torr vacuum conditions). Cs_2Te is less sensitive to contamination than alkali-antimonide photocathodes. In addition, it has a comparatively shorter response time (~ ps), a higher current density and a lower dark current than most other semiconductor photocathodes.

At ASTeC, the operation of CLARA has been based on metal photocathodes, however, for the future operation as a FEL injector, there is need to produce photocathodes based on Alkali-telluride. For that purpose, we have designed a new photocathode preparation facility, capable of producing a variety of photocathodes ranging from metal, metal/oxide, and caesium implanted metal to Alkali-telluride/antimonide. The versatility of the system is based on the ion beam deposition and ion beam implantation. We will report on the synthesis of Cs_xTe photocathodes, both in concurrent and sequential mode.

CATHODE PREPARATION

Molybdenum foil, 0.5 mm thick, is cut into disks and degreased in acetone, methanol and deionised water sequentially in an ultrasonic bath. The disks are dried and clamped into self-heating stubs and then introduced into a load lock, which is baked overnight, to bring the base pressure in 10^{-9} mbar. The Mo substrate is transferred on a linear sample drive, into the analysis chamber, where it is ion beam sputter cleaned to remove all oxides and carbon from the surface. Next, it is transferred to the deposition chamber and is placed onto the sample holder with the wobble stick. The

ISBN: 978-3-95450-227-1 ISSN: 2673-5490 doi:10.18429/JACoW-IPAC2022-MOPOMS027

targets are placed on a circular disk, at the edge of which, 5 targets holders, are mounted at 45-degrees as shown in Fig. 1. The targets are electrically isolated, so that the sputtering current can be monitored during the deposition. The secondary electrons emitted from the target during sputtering are not suppressed.

The target wheel is rotated to place the required target (Te) in the top position facing the ion source; this can then be driven in so that it is above the sample position. The Te deposition is done by ion beam sputtering. The ion gun accelerates ions into the Te target, causing sputtering onto the sample. The deposition rate is controlled via ion current, ion energy and the distance between the target and the substrate. After use, the target holder is withdrawn to allow the linear sample drive to pass it. The evaporation sources (Cs) can be degassed in the withdrawn position and then driven towards the sample to coat it. Cs deposition rate is estimated from the table provided by SAES getters. After use, the source is withdrawn.

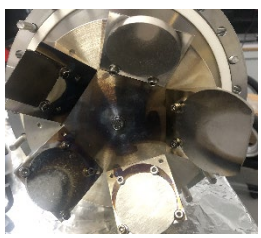

Figure 1: Arrangement of target wheel.

For concurrent deposition, the Te deposition and Cs evaporation were carried out at the same time. For Te deposition, a Kr ion beam of 5 keV energy, a current of 40 µA and a working pressure of 10^{-5} mbar was used. The target to substrate distance was ~3 cm. The Te film thickness is estimated to be about 20 nm. The estimation is done on the basis of the XPS analysis depth which is 10 nm. The deposition time was set to be twice the time when substrate signal is not detectable. For Cs deposition the evaporation current was set to 5.55 A at a voltage of 1.82 V. The substrate was held at 120 C. The Cs source to substrate distance was 4 cm. In the case of sequential deposition, Te was first deposited for 1 hour, using ion beam sputtering deposition. The fresh film was analysed by XPS and then returned into the deposition chamber, where it was exposed to Cs vapour with the same parameters as for the co-deposition, of 1 hour at 120 C. For quantum efficiency measurement, a 266 nm UV LED is mounted behind a UV transmission window, on a Z-drive, behind an inline valve. The transmission window is recessed by 10 mm inside a mini flange. This recessed gap can act as Faraday cup for measuring the photocurrent. The power of the UV diode was determined by a calibrated power meter placed at the same position of the substrate. The measured power was 0.3 mW. The quantum efficiency is then calculated using the following formula:

$$QE = \frac{ne}{n\gamma} = \frac{Ihc}{e\,P\gamma\lambda} \quad (1)$$

where nγ is the number of incident photons, ne is the number of electrons generated by the incident photons, I is photocurrent, e is electric charge, Pγ is the ultraviolet irradiance of the cathode surface, λ is the wavelength of the incident ultraviolet light, h is the Planck constant, and c is the velocity of light.

The sample was then analysed by XPS to determine its composition and chemical state. For analyses, aluminium, monochromatic X-rays with a beam spot of 650 µm and a VG alpha 110 hemispherical analyser were used. The survey spectra were collected at 50 eV pass energy, whilst for region spectra, a pass energy of 20 eV was employed. For data analyses, Advantage processing program provided by VG was used.

RESULTS

Figure 2 (b) depicts the surface chemical state of the as received moly substrate. The dominant peak in the survey spectra is O1s and C1s. In contrast, for the Kr sputtered clean Mo, the dominant peak is associated with metallic Mo peaks. This is further illustrated from the region spectra of Mo3d as shown in Fig. 2 (a). The doublet Mo3d associated with MoO_3 for j = 5/2 at binding energy of 232.7 eV and j=3/2 at binding energy of 236.1 eV has completely disappeared after Kr ion beam cleaning.

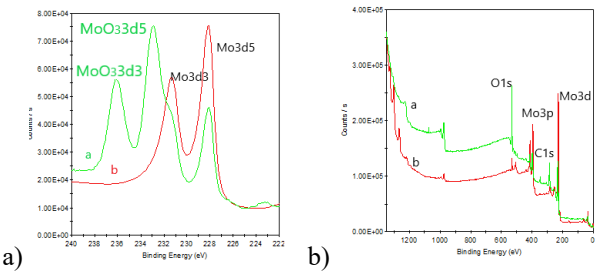

a) b)

Figure 2: overlay XPS spectra of sputtered clean and as received moly sample. a) Mo3d scan and b) survey scan.

Figure 3 shows the overlay of survey spectra of the CsTe synthesised in co-deposition and sequential mode as well as the intial Te deposition. . The composition at the surface layer is calculated using normalised area and smart background subtraction. The smart background option is based on the Shirley background with additional constraint that the background not to be of a greater intensity than the actual point in the region. This makes the calculated background not sensitive to the selection of the background. The normalised area is calculated by dividing the peak area by transmission function, sensitivity factor and energy compensation factor. The overall composition using region area of respective elements is calculated to be Cs_2Te and Cs_3Te for co-deposition and sequential deposition respectively.

For 3d3/5, these are at binding energy of 571.2 eV corresponding to Cs_2Te; at binding energy of 573 eV corresponding to metallic Te; and binding energy of 576 eV corresponding to TeO_2 (Te^{+4}). Figure 4 (b) compares the Te3d region taken with the sample being at 0 degree to the analyser normal, and when the sample is at 60° to the analyser normal.

ISBN: 978-3-95450-227-1 ISSN: 2673-5490 doi:10.18429/JACoW-IPAC2022-MOPOMS027

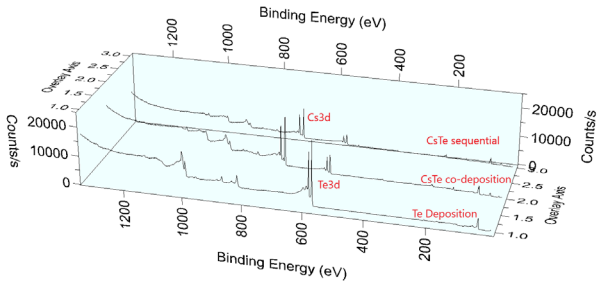

Figure 3: Survey spectra using Al monochromatic X-ray of co-deposited and sequential deposition of Cs_xTe film on Moly substrate. With pass energy of 50 eV. The Te deposition is also included for comparison.

The later will sample a shallower region of the film surface. The ratio of j = 5/2 of Te^0:Te^{-2} for 0° to 60° decreases from 2.15 to 1.34. This implies that the Cs_2Te phase is at the surface. Figure 4 (c) and (d) depict the Te3d region for CsTe sample deposited in sequence and the overlay of all Te3d of deposited films respectively. In contrast to the co-deposited sample no oxygen contamination is present either in pure Te deposition nor in sequential Cs_xTe sample. The 3d spin orbit coupling is a single peak at binding energy of 573 and 571.9 eV for j = 5/2 and at binding energy of 583.4 and 582.3 for j = 3/2 for pure Te and CsTe, respectively. The Te3d5/2 peak can be de-convoluted into three peaks centred at 571.2 eV, 571.9 eV and 572.8 eV.

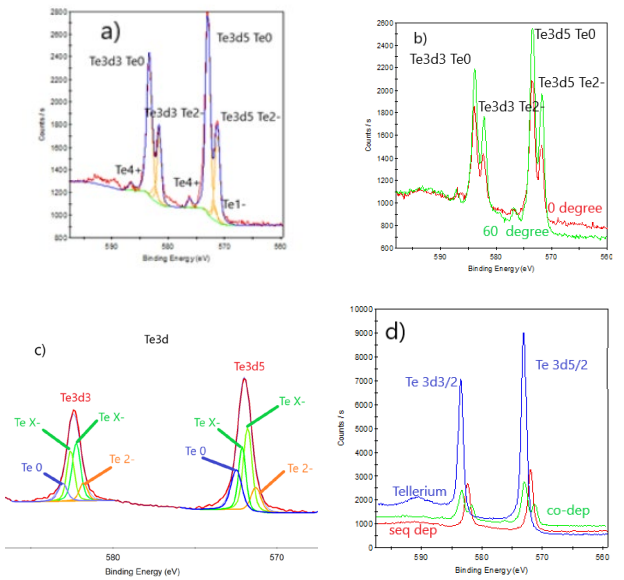

Figure 4: Region spectra of Te3d using Al monochromatic X-ray of Cs_xTe film on Moly substrate, with pass energy of 20 eV: a) co deposited sample at 0 degree to analyser normal, b) overlay of 0° and 60° angle to analyser normal, c) sequential deposition sample, d) overlay of Te and Cs_xTe. Figure 5 shows the photocurrent I_{ph} emission for various extraction voltage when photons with λ = 266 nm irradiates the sample surface. Based on Eq. (1), for 0.3 mW power, photoemission (I_{ph}) of 1 µA corresponds to a QE of 1.55%. At the saturation level of 4.8 and 6.3 µA the QE corresponds to 7.5 and 9.7% for co-deposited and sequential deposition, respectively.

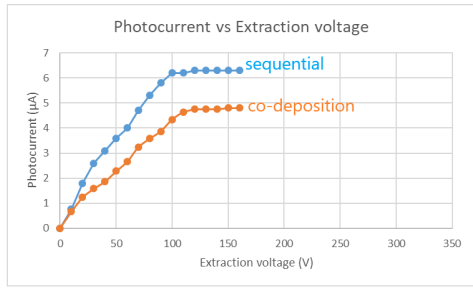

Figure 5: Measured photocurrent as a function of extraction voltage using 266 nm radiation from a UV laser diode.

DISCUSSION

Both co-deposition and sequential deposition of Cs and Te resulted in mixed phase Cs_xTe. The XPS spectra of the Te3d region show a doublet, due to spin orbit coupling with both j = 5/2 and j = 3/2, with peaks at binding energies of 573 eV and 583.4 eV. The $Te3d_{5/2}$ at E_b = 571.2 eV corresponds to Cs_2Te as reported by various investigators. The deconvolution of the peaks also shows another small peak at E_b = 571.7 eV, which is assigned to Cs_xTe where $1< x < 2$. The peak at E_b = 576 eV is assigned to tellurium oxide TeO_2. The relative low QE 7.5 and 9% can be due to the lack of single phase Cs_2Te.

XPS survey spectra revealed the presence of a small but significant peak of Mo, which in the case of sequential deposition, was not present, prior to the Cs evaporation. This may be due to inducement of porous structure during the formation of the alloy phase or loss of original Te thickness. Ion beam sputtering usually produces uniform and dense film due to the extra energy of sputtered atoms, which is in the region of 6 to 10 eV. Further measurement needs to be carried out to elucidate the origin of surface morphology after Cs_xTe phase formation. Nevertheless, in both cases a reasonable QE is achieved despite the presence of oxygen in the co-deposited film. The origin of the contamination may be due to the initial outgassing stage of the Cs evaporation sources. The sequential mode was carried out after the co-deposition, by when the source was well conditioned. The ion beam sputtering is a very convenient and highly controllable PVD deposition process. Once the sputtering yield is stablished, the control of the deposition rate can be easily controlled by deposition parameters such as ion energy, ion bean flux and target substrate distance. The uniformity of the film can be easily controlled by the size and shape of the ion beam on the target.

CONCLUSION

We have synthesised Cs_xTe photocathodes by using ion beam sputtering and Cs evaporation. The method has a high degree of reproducibility. The purity of the film depends on the quality of the vacuum, the working gas and the purity of the target.

ISBN: 978-3-95450-227-1 ISSN: 2673-5490 doi:10.18429/JACoW-IPAC2022-MOPOMS027

REFERENCES

[1] J.A Clarke *et al.*, "CLARA conceptual design report", *Journal of Instrumentation*, vol. 9, no. 05, p. T05001, 2014.

[2] S.H. Kong *et al.*, "Photocathodes for free electron lasers", *Nucl. Instrum. Methods Phys. Res., Sect. A*, vol. 358, pp. 272-275, 1995. doi:10.1016/0168-9002(94)01425-6

[3] S. Lederer, F. Brinker, L. Monaco, S. Schreiber, and D. Sertore, "Update on the Photocathode Lifetime at FLASH and European XFEL", in *Proc. FEL'19*, Hamburg, Germany, Aug. 2019, pp. 427-429. doi:10.18429/JACoW-FEL2019-WEP047

[4] D. Sertore *et al.*, "First operation of cesium telluride photocathodes in the TTF injector RF gun", *Nucl. Instrum. Methods Phys. Res., Sect. A*, vol. 445, pp. 422-426, 2000. doi:10.1016/S0168-9002(00)00095-4

[5] P. Michelato, "Photocathodes for RF photoinjectors", *Nucl. Instrum. Methods Phys. Res., Sect. A*, vol. 393, pp. 455-459, 1997. doi:10.1016/S0168-9002(97)00545-7

[6] D. Bisero *et al.*, "High efficiency photoemission from Cs-K-Te", *Applied Physics Letters* vol. 70, p. 1491, 1997. doi: 10.1063/1.118362

[7] S.H. Kong *et al.*, "Fabrication and characterization of cesium telluride photocathodes: A promosing electron source for the Los Alamos Advanced FEL", *Nucl. Instrum. Methods Phys. Res., Sect. A*, vol. 358, pp. 276-279, 1995. doi: 10.1016/0168-9002(94)01279-2

[8] A. Fry, E. Hahn, W. Hartung, M. Kuchnir, P. Michelato, and D. Sertore, "Experience at Fermilab with High Quantum Efficiency Photo-Cathodes for RF Electron Guns", in *Proc. LINAC'98*, Chicago, IL, USA, Aug. 1998, paper TU4101, p.642.

[9] J. Teichert *et al.*, Report on photocathodes 2004.